

# Geophysical Research Letters®

## RESEARCH LETTER

10.1029/2022GL100886

### Key Points:

- Different crater morphologies between the lunar maria and the highlands were revealed from a new global catalog of lunar impact craters
- A global power-law relationship with an offset term was identified between crater depth-to-diameter ratios and crater densities
- Crater morphologies provided implications on different thicknesses and properties of the mare basalts and highland upper megaregolith

### Correspondence to:

B. Wu and Y. Wang,  
[bo.wu@polyu.edu.hk](mailto:bo.wu@polyu.edu.hk);  
[yiran.wang@connect.polyu.hk](mailto:yiran.wang@connect.polyu.hk)

### Citation:

Wu, B., Wang, Y., Werner, S. C., Prieur, N. C., & Xiao, Z. (2022). A global analysis of crater depth/diameter ratios on the Moon. *Geophysical Research Letters*, 49, e2022GL100886. <https://doi.org/10.1029/2022GL100886>

Received 8 DEC 2021

Accepted 17 OCT 2022

### Author Contributions:

**Conceptualization:** Bo Wu

**Formal analysis:** Bo Wu, Yiran Wang, Stephanie C. Werner, Nils C. Prieur, Zhiyong Xiao

**Funding acquisition:** Bo Wu

**Investigation:** Bo Wu, Yiran Wang





**Methodology:** Bo Wu

**Resources:** Bo Wu

**Writing – original draft:** Bo Wu

**Writing – review & editing:** Bo Wu, Yiran Wang, Stephanie C. Werner

## A Global Analysis of Crater Depth/Diameter Ratios on the Moon

Bo Wu<sup>1</sup> , Yiran Wang<sup>1</sup>, Stephanie C. Werner<sup>2</sup> , Nils C. Prieur<sup>2</sup> , and Zhiyong Xiao<sup>3</sup> 

<sup>1</sup>Research Centre for Deep Space Explorations, Department of Land Surveying and Geo-Informatics, The Hong Kong Polytechnic University, Kowloon, Hong Kong, <sup>2</sup>Department of Geosciences, University of Oslo, Oslo, Norway, <sup>3</sup>Planetary Environmental and Astrobiological Research Laboratory, Sun Yat-sen University, Zhuhai, P.R. China

**Abstract** On the Moon, the old anorthositic highland rocks and younger basaltic mare units show distinguishable differences in appearance. The craters on the lunar highlands and maria also show variation in morphological characteristics. We analyzed the crater morphologies on a global scale, based on our new global catalog of lunar impact craters ( $\geq 1$  km in diameter) with morphological information for each crater. We find that there is a global power-law relationship with an offset term between crater depth-to-diameter ratios and crater densities. Small craters (less than  $\sim 4$  km in diameter) on the lunar maria are found to be deeper than those on the highlands, indicating differences in target properties and crater degradations. Furthermore, the depths of the deepest simple craters identified on the lunar maria and the highlands provide references that the mare basalts and highland upper megaregolith have thicknesses of  $\sim 2.3$  and  $\sim 3.3$  km, respectively.

**Plain Language Summary** The lunar surface is divided into light areas called lunar highlands and darker areas called maria. The craters show variation in morphological characteristics on the lunar highlands and maria. The depth-to-diameter ratios reflect the morphological characteristics of craters. Global distribution of crater depth-to-diameter ratios in different diameter ranges are analyzed. We find that there is a global power-law relationship with an offset term between crater depth-to-diameter ratios and crater densities. Small craters (less than  $\sim 4$  km in diameter) on the lunar maria are found to be deeper than those on the highlands, which indicates differences in target properties and crater degradations. Furthermore, the depths of the deepest simple craters identified on the lunar maria and the highlands provide references that the upper layer of the maria and highlands have thicknesses of  $\sim 2.3$  and  $\sim 3.3$  km, respectively.

## 1. Introduction

On the Moon, the old anorthositic highland rocks and younger basaltic mare units show distinguishable differences in appearance. The craters on the lunar highlands and maria also show variation in morphological characteristics, which indicate differences between the crater degradation status (e.g., Fassett & Combellick, 2014), the stratified geological layers (e.g., Du et al., 2019; Melosh, 1977; Pike, 1981; Richardson & Abramov, 2020), the properties of the target materials (e.g., Prieur et al., 2017; Senft & Stewart, 2007), or a combination of these factors.

The global distribution and morphological characteristics of lunar impact craters provide important clues in the research of differences between lunar maria and highlands. Previous research on the global characteristics of lunar craters has mostly focused on planimetric attributes, such as crater size-frequency distributions (Neukum et al., 2001) and crater saturation (Xiao & Werner, 2015). The limited availability of three-dimensional (3D) morphological data has meant that 3D crater morphology studies have only been performed at local scales, such as the assessment of crater depth-to-diameter ratios at the Apollo landing sites (Pike, 1974; Wood & Anderson, 1978) or the examination of crater degradation in some lunar maria (Fassett & Thomson, 2014).

Recent lunar missions have collected high-resolution remote sensing data sets covering the entire lunar surface, from which global 3D products such as digital elevation models (DEMs) and orthoimage mosaics have been generated with higher spatial resolutions than were previously available. These DEMs include the Lunar Orbiter Laser Altimeter (LOLA) DEM (Smith et al., 2010) and the SELEnological and ENgineering Explorer (SELENE) and Lunar Reconnaissance Orbiter DEM (SLDEM; Barker et al., 2016), which offer effective spatial resolutions better than 512 pixels per degree ( $\sim 60$  m/pixel at the equator). In addition, the orthoimage mosaics generated from KAGUYA (SELENE) Terrain Camera (TC) images (Kato et al., 2008) and Chang'E-2 images (Li et al., 2018)



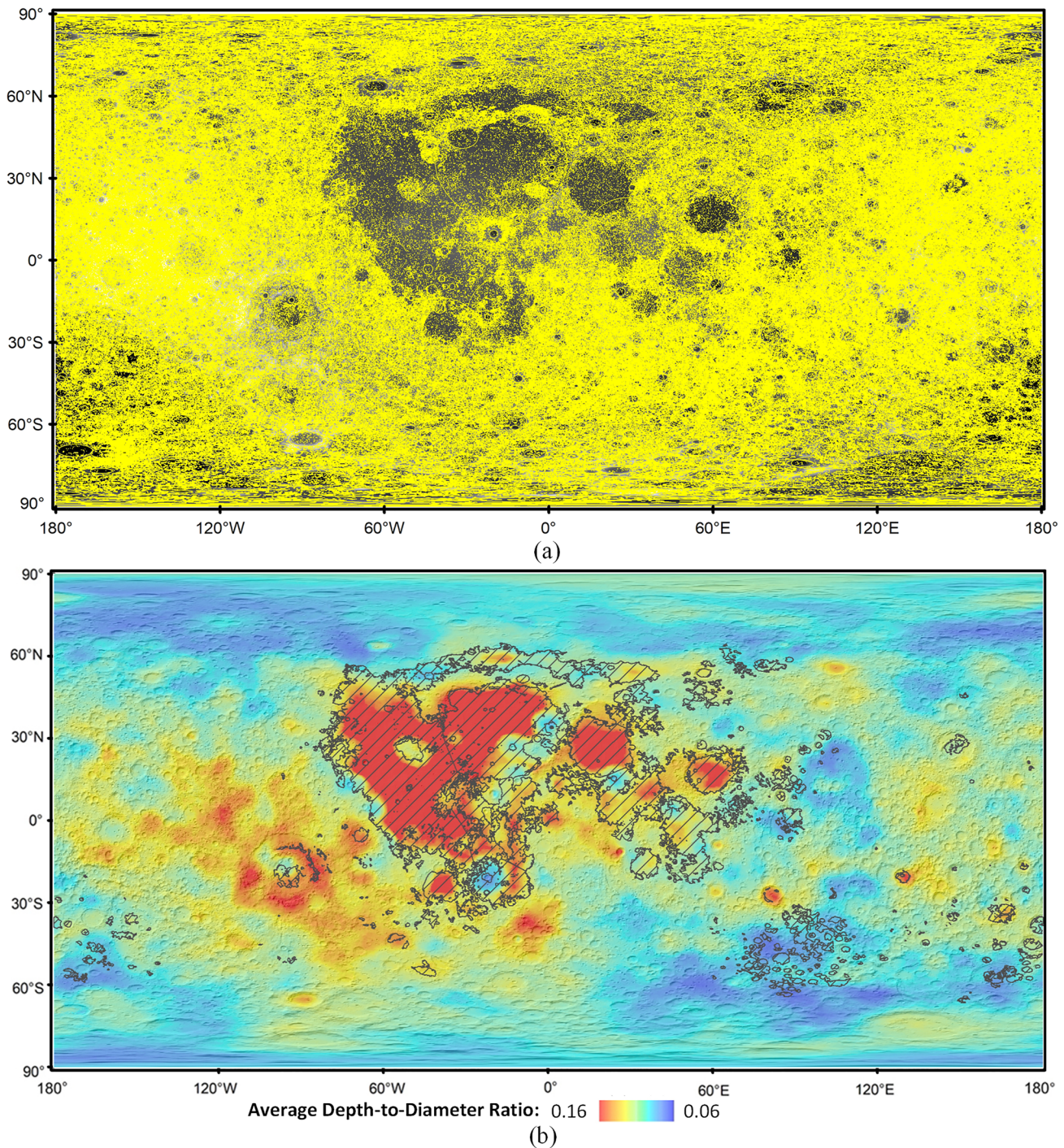


**Figure 1.** (a) Overview of the global catalog of lunar craters ( $\geq 1$  km), LU1319373 (Wang et al., 2021). Craters are outlined in yellow. (b) Global crater depth-to-diameter ratio map. Lunar mare regions are marked by gray hatching. It is worth noting that this depth-to-diameter ratio map is dominated by small craters ( $\sim 1$ – $2$  km in diameter) due to their overwhelming numbers (For larger craters, refer to Figure 2 for depth-to-diameter ratio maps in different diameter bins).

have spatial resolutions of better than 10 m/pixel. Based on these high-resolution data sets, we developed a new global catalog of lunar impact craters, LU1319373 (Wang et al., 2021), which contains approximately 1.32 million craters ( $\geq 1$  km in diameter), as shown in Figure 1a. Each entry includes the center coordinates, diameter, and 3D morphological information of a crater, such as its depth and rim height.



The global scale of this new crater catalog and its embedded 3D morphological information (to a minimum crater size of 1 km) offers new opportunities to investigate impact morphologies and the associated cratering processes on the lunar surface. Here we report the different crater morphologies between the lunar highlands and maria based on the new crater catalog, and new implications for the differences between lunar maria and highlands.

## 2. Data and Methods

A global catalog of lunar craters, LU1319373, was generated using a machine-learning algorithm for automatic crater detection from lunar DEMs, followed by extensive manual checking to global orthoimage mosaics (Wang et al., 2021). The machine-learning approach (Wang & Wu, 2019; Wang et al., 2021) includes a feature descriptor based on the histogram of oriented gradient (HOG), which describes the elevation changes of craters in the DEM, and a support-vector machine classifier that was trained and optimized on the HOG features from thousands of positive samples (craters) and negative samples (non-craters). A global DEM, comprised of the SLDEM covering  $-60^{\circ}$  to  $60^{\circ}$  latitude and the LOLA DEM covering higher latitudes, was fed to the well-trained classifier to detect craters and output their center coordinates and diameters. The SELENE TC and Chang'E-2 image mosaics were used to assist in manual checking of the classifications. A grid with a cell size of  $1 \times 1$  km was overlaid on the images and the DEM data to help validate the automatic detection results and identify any missed craters. Verification was also performed against previously published catalogs (Head et al., 2010; Robbins, 2019). The verification efforts were conducted by a group of independent operators to ensure the reliability of the crater-detection results.

To measure the depth parameter for each crater, north-south and east-west profiles were derived from the DEM for each detected crater. The crater depths were then determined as the averages of the vertical distances between the rim crest to the crater floor, which was derived from each profile. The performance of this method was validated by comparing the derived crater depths with the manually measured depths, which revealed an average depth deviation of approximately 0.5% of the crater diameter. Details can be found in our previous publication (Wang et al., 2021).

## 3. Results

### 3.1. Global Crater Depth-To-Diameter Ratios

Crater depth is defined as the vertical distance from the floor of a crater to its rim height, and is related to the magnitude of the original cratering impact and affected by the subsequent evolution of the crater (Barnouin et al., 2012). The statistical relationships between crater depths and diameters, which are commonly defined by depth-to-diameter ratios, have been useful for formulating models of the post-impact degradation and modification of craters (Pike & Spudis, 1987). Investigations of crater depth-to-diameter ratios have also provided quantitative evidence of transitions from simple to complex crater morphologies (Wünnemann & Ivanov, 2003).

To evaluate the spatial associations between crater depth-to-diameter ratios and crater locations on the lunar surface, we derived the average depth-to-diameter ratios of various diameter ranges of craters, which resulted in global crater depth-to-diameter ratio as shown in Figure 1b. The depth-to-diameter ratio maps are calculated using 100-km-radius circular moving windows for craters of 1–16 km and 300-km-radius circular moving windows for craters >16 km. The size of moving windows is in geodetic distances and the same hereafter. The maps showed that the average depth-to-diameter ratios of craters range from 0.06 to 0.16, and the spatial distribution of craters with particular ratios revealed that there are differences between the morphology of craters on the lunar maria and those on the highlands. Specifically, most lunar mare regions have average crater depth-to-diameter ratios greater than 0.1, whereas most highland regions have average crater depth-to-diameter ratios lower than 0.1.

It is worth noticing that the depth-to-diameter ratio map as shown in Figure 1b is dominated by small craters ( $\sim 1$ –2 km in diameter) due to their overwhelming numbers. Thus, to clarify the depth-to-diameter ratios of craters in different diameters, Figure 2 shows detailed crater depth-to-diameter ratio maps binned using six diameter ranges. The depth-to-diameter ratio maps for craters 1–16 km in diameter were calculated using 100-km-radius circular moving windows. Larger moving windows of a 300-km-radius were adopted for craters >16 km, as larger craters are fewer in numbers and more sparsely distributed. In general, craters up to 8 km in diameter on the lunar maria are deeper than the same-sized craters on the highlands, but the distinction is far less pronounced

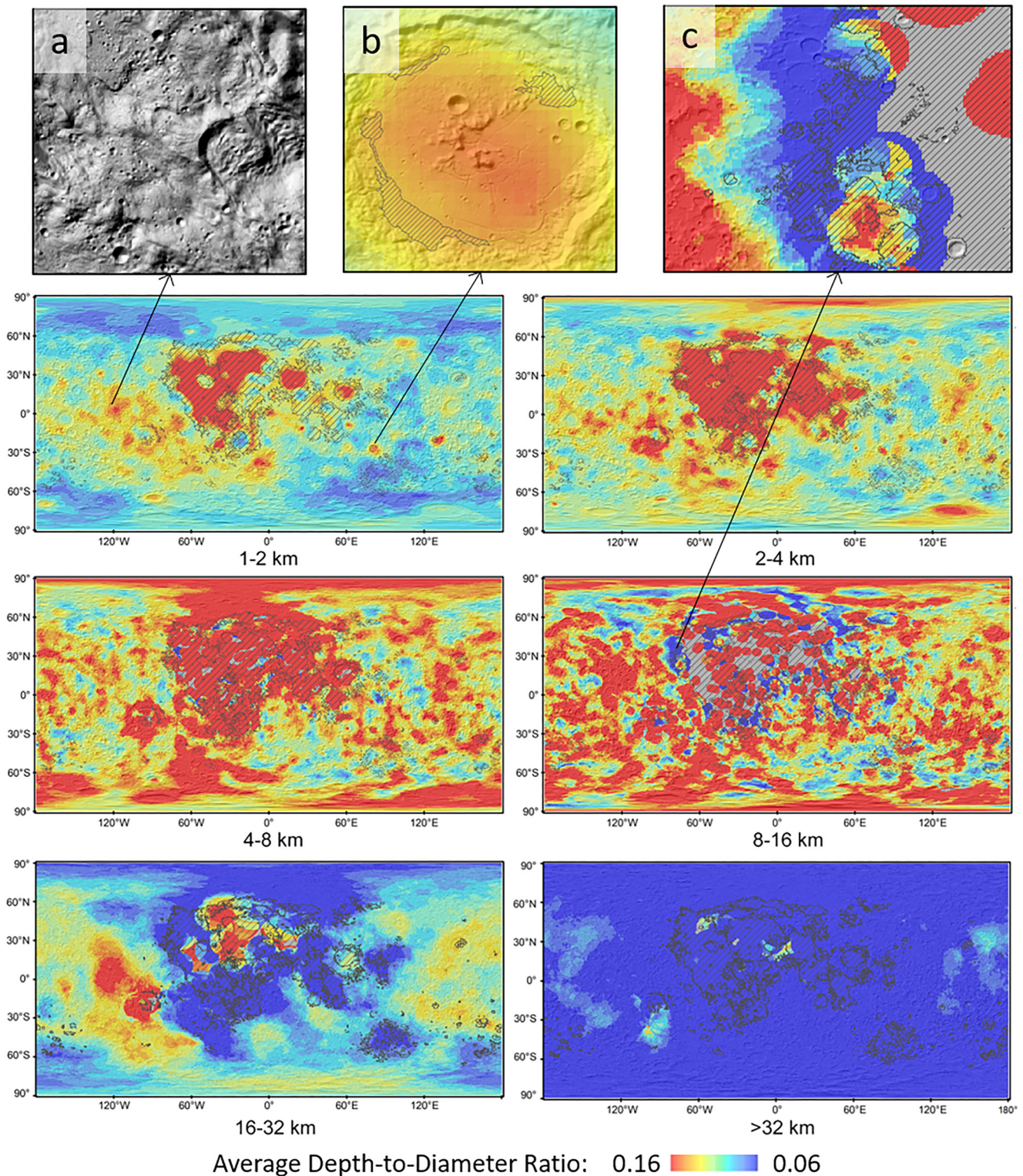


**Figure 2.** Global crater depth-to-diameter ratio maps calculated for six diameter bins. The maps for craters of 1–16 km and >16 km are calculated using 100-km–radius and 300-km–radius circular moving windows, respectively. Lunar mare regions are marked by gray hatching. The enlarged views on the top show examples of (a) deep craters located on the ejecta of large impact basins, (b) deep craters located on the impact-melt floors of larger craters, and (c) shallow craters at the borders between mare and highland units.



than those in previous studies (Pike, 1974, 1981), which examined only apparently fresh craters. This discrepancy with previous studies is mainly due to crater degradation, as we included both fresh and old craters. In addition, there are a large number of deep craters within the smallest diameter range (1–2 km) in the highland units. These deep craters are typically located on the impact-melt floors of larger craters (see an example of region “b” in Figure 2) or on the ejecta of large impact basins (see an example of region “a” in Figure 2). Highland craters in this diameter range are mostly in equilibrium saturation (Xiao & Werner, 2015).

We also found apparent latitudinal variations in the crater depth-to-diameter ratios, which are generally shallower at higher latitudes ( $>60^\circ$ ). For the diameter range (1–2 km), the regions with a latitude less than  $60^\circ$  have an average depth-to-diameter ratio of 0.084, which is 16.7% higher than the average ratio of 0.072 for regions with latitudes higher than  $60^\circ$ .

The distinction between maria and highland craters is most prominent in the next diameter range (2–4 km), with deeper craters present in the mare areas. This may suggest that the craters in 2–4 km in highlands are more easily degraded. The distinction is less in the 4–8 km diameter range, and absent in the 8–16 km diameter range. The less distinction in depth-to-diameter ratio maps at larger diameters can be explained by the phenomenon that crater degradation is less pronounced with the increasing diameter (Basilevsky et al., 2018; Fassett et al., 2017). In larger diameter bins there are very few craters in the mare areas, and craters with diameters larger than 32 km have low depth-to-diameter ratios in general.

The greatest changes in crater morphologies are seen in the 8–16 km and 16–32 km diameter ranges, in which shallow craters are commonly observed at the borders between mare and highland units (see an example of region c in Figure 2). The distribution of these shallow craters could be due to basaltic flooding along the mare-highland boundaries (described in detail in the following section).

### 3.2. Relationships Between Crater Morphology and Crater Density

Analysis of our new catalog revealed apparent relationships between crater morphology and crater density. The crater density map presented here in Figure 3a was derived from the new catalog by counting the number of craters in a 100-km-radius circular moving window. Figures 3a and 3b show a direct comparison of the crater depth-to-diameter ratio map and the crater density map, of which four areas of particular interest are highlighted using different colors. The two regions outlined by the red boundary and the yellow boundary, respectively, are characterized by higher-than-average depth-to-diameter ratios. The area within the red boundary approximately corresponds to the extent of the lunar mare on the nearside, and that within the yellow boundary outlines the Orientale Basin and the surrounding region. The corresponding crater-density maps reveal lower-than-average crater densities within these two regions. This inverse relationship between depth-to-diameter ratios and crater densities arises because these two regions are the most recently resurfaced terrains on the Moon, and have thus been subjected to the shortest period of impact crater accumulation and degradation.

In contrast, the two regions outlined by the blue boundary (encompassing the north pole of the Moon) and the green boundary (a local region  $\sim 10^\circ$ – $90^\circ$ E,  $\sim 10^\circ$ – $60^\circ$ S), respectively, have the opposite relationship: lower-than-average depth-to-diameter ratios but higher-than-average crater densities. This may be because these regions have experienced extensive impacts, and the resulting craters have had sufficient time to degrade in shape and decrease in depth compared to fresher examples. It is also possible that these regions have large numbers of secondary craters, such as the craters clustered in radial distribution patterns in Figure 3b. These secondary craters have relatively high spatial densities and low depth-to-diameter ratios. Other potential causes for the low depth-to-diameter ratios may relate to the distribution of materials of various strengths and a dependency of crater degradation on physical properties (Schultz et al., 1977).

Figure 3c presents a pixel-by-pixel plot of the relationship between the crater depth-to-diameter ratio map and the crater density map. The colors of the dots correspond to the regions marked in Figures 3a and 3b. Hence, the red dots and yellow dots are distributed in the upper left of the plot, indicating greater depth-to-diameter ratios and lower crater densities, whereas the blue dots and green dots are distributed in the lower right of the plot, indicating lower depth-to-diameter ratios and higher crater densities. The black dots represent pixels outside the marked regions.

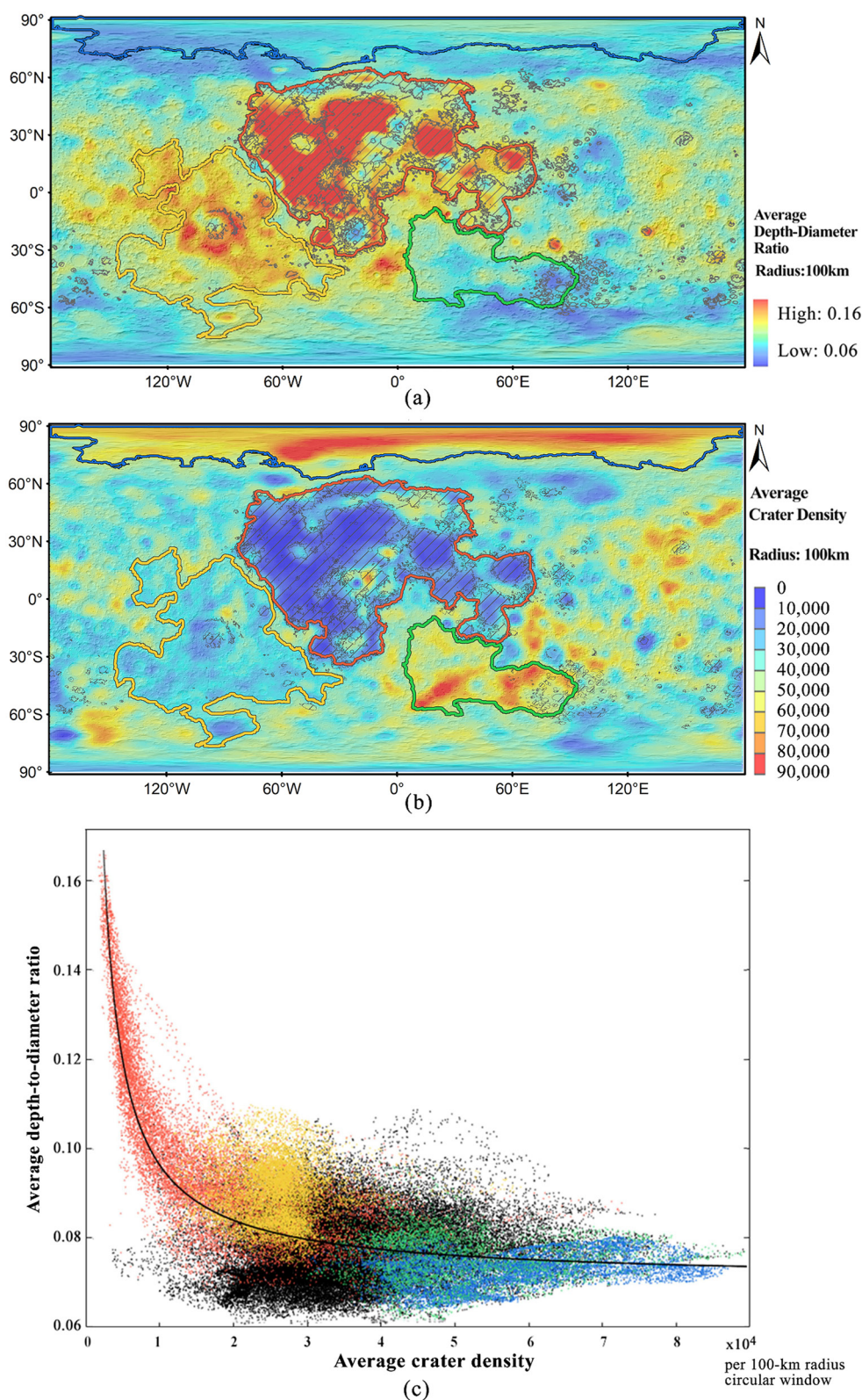


Figure 3.



It can be seen from Figure 3c that the relationship between the crater depth-to-diameter ratio and the crater density generally follows a power-law distribution with an offset term. We used a least-squares fitting method to determine the best fitting of a power-law function, which is as follows:

$$d/D = 133.6N^{-0.926} + 0.07, \quad (1)$$

where  $N$  is the crater density, and  $d/D$  is the average crater depth-to-diameter ratio, both of which were calculated in a 100-km-radius circular moving window. The fitting has an  $R$ -square value of 0.56, showing a good fit at the start and end parts, but relatively scattered in the middle (Figure 3c). This power-law function can be used for the general estimation of lunar-crater densities from crater morphologies, and vice versa. As the depth-to-diameter ratio map and density map in Figure 3 are dominated by small craters ( $\sim 1$ – $2$  km in diameter) due to their overwhelming numbers, this function has the highest credibility for craters in this diameter range.

Figure 3c and the power-law fitting indicate that surfaces with larger crater densities generally have smaller depth-to-diameter ratios. The surfaces (lunar mare) with crater densities of less than  $\sim 2 \times 10^4$  craters (diameters  $\geq 1$  km) per unit (100-km-radius circular window) have obviously larger average depth-to-diameter ratios (up to 0.16). This implies that deeper craters tend to be located in younger surfaces (i.e., lower crater density), where these craters have not been significantly modified by degradations. The plots for the Orientale Basin and its surrounding region (in yellow) have crater densities of  $\sim 2$ – $3 \times 10^4$  per unit and average depth-to-diameter ratios of  $\sim 0.08$ – $0.11$ , which represent an inflection point. For the surfaces (e.g., the north pole) with crater densities  $> 3 \times 10^4$  per unit, their average depth-to-diameter ratios are relatively constant and converge to  $\sim 0.07$  (refer to the offset term in Equation 1). Previous research classified the crater degradation states into two stages: (a) “sandblasting,” for low crater density regions where large craters were gradually erased by smaller craters over time; and (b) “cookie-cutting,” for high crater density regions where the surfaces were frequently reset by the formation of large craters (Richardson, 2009; Woronow, 1977a, 1977b, 1978). Due to the intensive bombardment, “cookie-cutting” might be the dominant process prior to the formation of the Orientale Basin, causing crater populations to reach equilibrium (Werner, 2014; Xiao & Werner, 2015). The “cookie-cutting” might terminate the downward trend of crater depths in high-density regions, as the impact process removed the craters directly, instead of shallowing the craters by sputtering. This may explain why the average depth-to-diameter ratios drop quickly at lower density and become relatively constant at high-density regions, with the plots from the Orientale Basin as the turning point. The convergence value of 0.07 may suggest the average depth-to-diameter ratio on saturated surfaces.

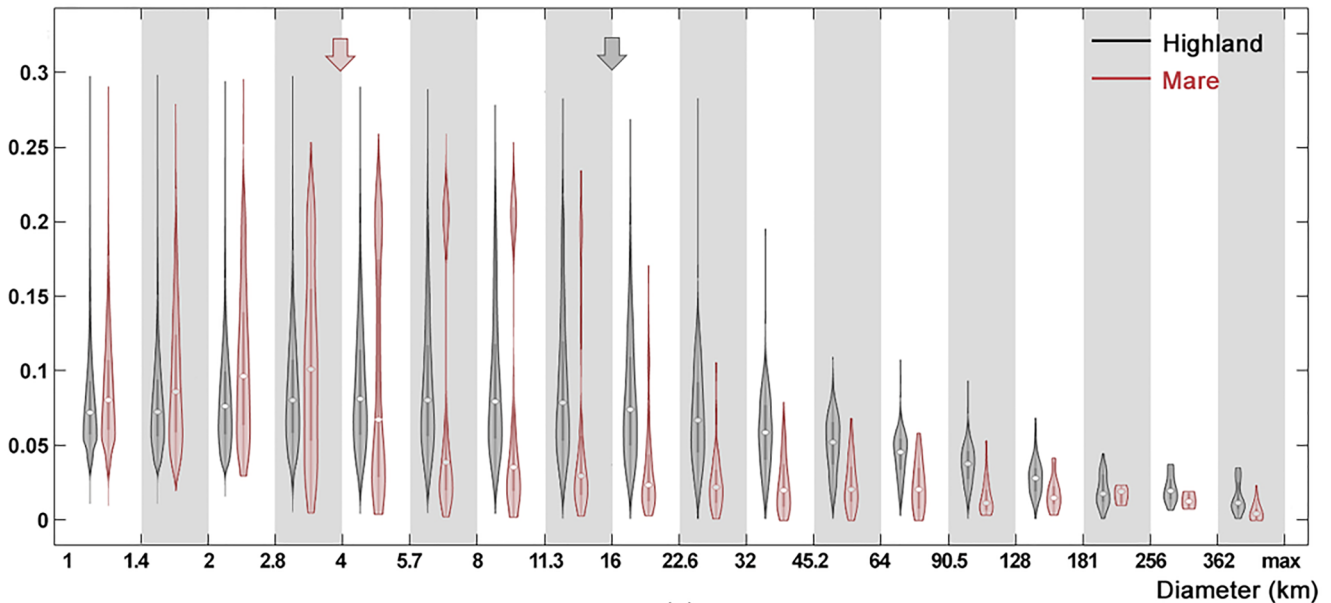
### 3.3. Morphometric Differences Between Craters in the Highlands and the Maria

It has been suggested that there are morphometric differences between craters in the lunar highlands and those in the maria. Previous studies noted that complex craters on highland terrain appear to be deeper than those on the mare (Kalynn et al., 2013; Pike, 1981; Wood & Anderson, 1978). The current study of our new higher-resolution global crater data set suggests that some modifications can be made to these previous suggestions. Figure 4a shows a violin plot of crater depth-to-diameter ratios in different diameter ranges for all of the cataloged craters ( $\geq 1$  km diameter) in the lunar highlands and the maria. It is worth mentioning that the mare craters include craters flooded by lava flows related to mare volcanism after their formation. This will be discussed in detail later. As can be seen, there are distinct differences between the two distributions, although the full range of the observed depth-to-diameter ratios in the two units do overlap substantially in the diameter ranges below approximately 15 km and above approximately 180 km. A similar phenomenon was previously observed by Pike (1974) in an analysis of the Moon's simple (well-preserved) craters.

Figure 4a indicates that small diameter ( $< 4$  km) craters are generally deeper relative to their diameters in the lunar maria than in the highlands. Conversely, larger-diameter craters are generally deeper relative to their diameters in the highlands than in the maria. Kalynn et al. (2013) suggested that the fragmented and porous megaregolith might allow the formation of deeper craters in the highlands. For why the small craters ( $< 4$  km) in the lunar

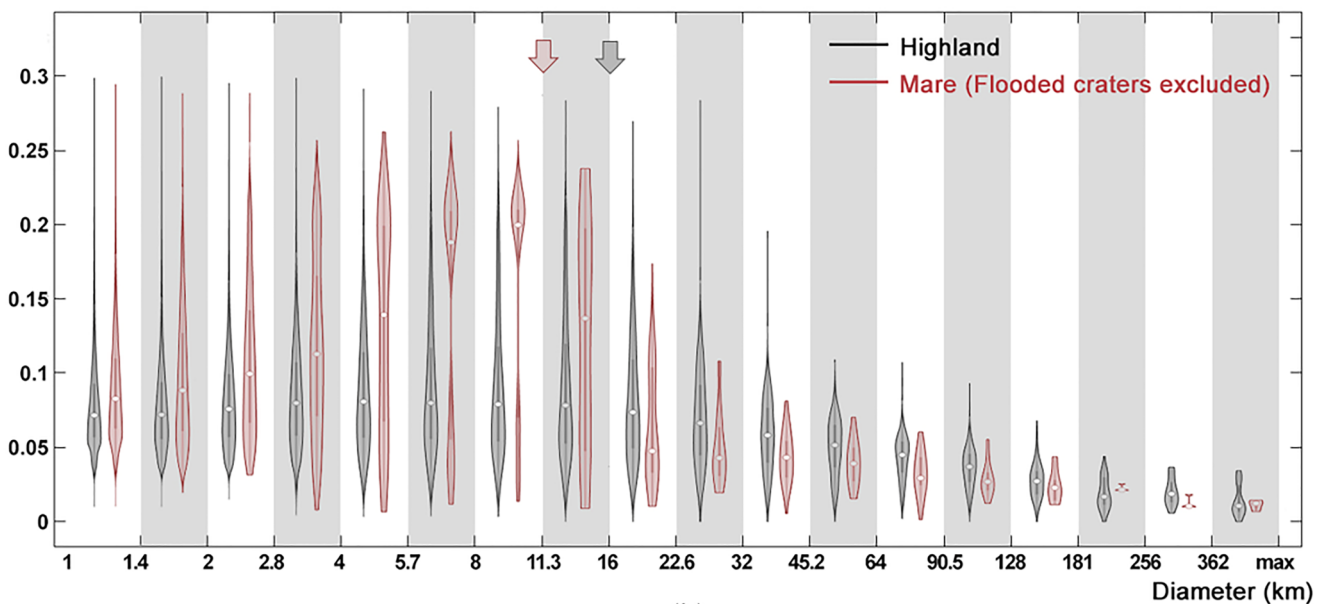
**Figure 3.** Relationships between crater depth-to-diameter ratios and crater densities. (a) Crater depth-to-diameter ratio map ( $\geq 1$  km in diameter) with four areas of specific interest highlighted by red, yellow, blue, and green boundaries, calculated using a 100-km-radius circular moving window. (b) Crater density map ( $\geq 1$  km in diameter) with the same four regions marked, calculated using a 100-km-radius circular moving window. (c) Correlation plot of all of the pixels in the two maps. The pixel colors correspond to the four regions marked in (a) and (b). The black dots represent pixels outside the highlighted regions. The black line is the power-law function described by Equation 1.

Depth-to-Diameter Ratio



(a)

Depth-to-Diameter Ratio



(b)

**Figure 4.** Violin plots of depth-to-diameter ratios for craters. (a) All craters on the highlands (black) and on the maria (red). (b) All craters on the highlands (black) and post-mare craters (craters largely flooded by lava flows are excluded) on the maria (red). In each diameter range, wider sections of the violin plot represent a higher population on the given value and vice versa; the white dot represents the median; the thick bar in the center represents the interquartile range (75th percentile and 25th percentile). The arrows indicate the turning point from increasing to decreasing of the median crater depth-to-diameter ratios.

maria are deeper relative to their diameters than those in the highlands, there might be two interpretations: (a) small highland craters (<4 km) might be more severely degraded over time compared with those of similar sizes on the lunar maria, as the latter has younger surfaces (Melosh, 1989; Richardson, 2009; Xiao & Werner, 2015); and (b) the target properties of the lunar maria are more competent at depths of ~400 m. Figure 4a also shows that the median depth-to-diameter ratios for small craters in both the lunar maria and the highlands increase gradually with crater diameter, and then decrease after a certain threshold diameter. For the maria craters, this transition occurs at a diameter of approximately 4 km. At the same time the variation in the ratio increases, while



the median ratio decreases from above 0.1 to below 0.05. For the highland craters, this low median ratio of 0.05 only occurs in craters larger than 45 km in diameter. Overall, the median depth-to-diameter ratio of highland craters gradually increases up to a crater diameter of approximately 16 km, and thereafter decreases to an ultimate apparent ratio of 0.01 for the largest craters. The transition to median ratios of less than 0.05 is observed early in the mare craters, occurring once the crater diameters exceed 8 km.

In the above discussion of region c in Figure 2, it is mentioned that some shallow craters are commonly observed at the borders between mare and highland units. Those shallow craters could be due to flooding by lava flows related to mare volcanism after their formation; if so, it would mean that their current depth-to-diameter ratios are significantly smaller than they initially were. To exclude impact craters with severe post-formation modifications, we carefully checked the lunar mare craters in our catalog to identify those with obviously incomplete rim segments and flooded floors.

Accordingly, 1,643 largely flooded craters (not including those craters blanketed only by ejecta) were manually marked. These craters were found to have diameters ranging from 1 km (the lower limit of the catalog) to 257 km. Figure 5 shows examples of lava-flooded craters. These craters are commonly located along the boundaries between the lunar maria and the highlands, such as along the upper boundary of Oceanus Procellarum, as shown in the upper left of Figure 5a. This finding could indicate that mare layers are thinner at their boundaries than in their central basin areas, in agreement with previous research (e.g., Du et al., 2019; Thomson et al., 2009). In Figure 5c, the histogram of the flooded craters of different diameter ranges indicates that the lava infill has the greatest effect on the crater distribution in the 3–9 km diameter range. This statistical prominence of lava-flooded craters within a specific diameter range on the maria could mean that a crater's rim height relative to the thickness of the basaltic lava affects the crater's flooding potential. The relationship between crater rim height and the thickness of the basaltic lava has been studied previously (Baldwin, 1970; De Hon, 1974; Du et al., 2019; Head, 1982; Whitford-Stark, 1982). We further examined dozens of fresh (unflooded) craters on the lunar maria with diameters of approximately 3 and 9 km, respectively, and derived their rim heights for reference. The craters with diameters of approximately 3 km were found to have an average rim height of approximately 55 m, and the craters with diameters of approximately 9 km were found to have an average rim height of approximately 300 m. These measurements could indicate that the basaltic lavas in these mare boundaries have thicknesses of approximately 55–300 m. This range is slightly narrower than the range (33–455 m) obtained by Du et al. (2019), who used 41 mare craters with completely exposed rims to estimate the mare basalt thicknesses around mare boundaries.

The identified flooded craters on the lunar mare were then excluded in the analysis of crater depth-to-diameter ratios, and an updated violin plot is shown in Figure 4b. This increased the median depth-to-diameter ratio to approximately 0.2, and the turning point toward decreasing crater depth-to-diameter ratios with increasing crater size is not reached until craters are approximately 11 km in diameter. However, this turning-point diameter is still less than that for the highland craters (approximately 16 km). The variation of the depth-to-diameter ratios of the highland craters with diameters larger than approximately 45 km are larger than those of the mare craters of the same size, but the medians become similar. The similar medians may indicate that craters both on lunar maria and highland are impacting into the same deep crust at diameters of >45 km.

### 3.4. Implications of Crater Morphologies for the Layered Structure of the Lunar Crust

For both the lunar maria and highlands, the lunar crust is vertically stratified. The highlands are thought to be stratified into a regolith layer that overlies megabreccia and competent bedrock, which is called megaregolith (Melosh, 1977; Pike, 1981; Richardson & Abramov, 2020). The megaregolith is further stratified and is divided into three distinct regions (Richardson & Abramov, 2020): (a) a 5–20 m surficial regolith layer (Oberbeck & Quaide, 1968; Yue et al., 2019), consisting of loose, unconsolidated fines and breccia; (b) a 1–5 km upper megaregolith layer (Aggarwal & Oberbeck, 1979; Izquierdo et al., 2021), consisting of depositional layers of brecciated and/or melted material; and (c) a 20–25 km lower megaregolith layer (Wiggins et al., 2019), consisting of bedrock. The lunar maria has an extra layer (or multiple layers) of basalt on top of the megaregolith layer. This mare basalt layer consists of extrusive igneous rocks that are derived from partial melting of the mantle, and the thickness varies from several meters to several kilometers (e.g., De Hon, 1974, 1975, 1977; Du et al., 2019; Gong et al., 2016).

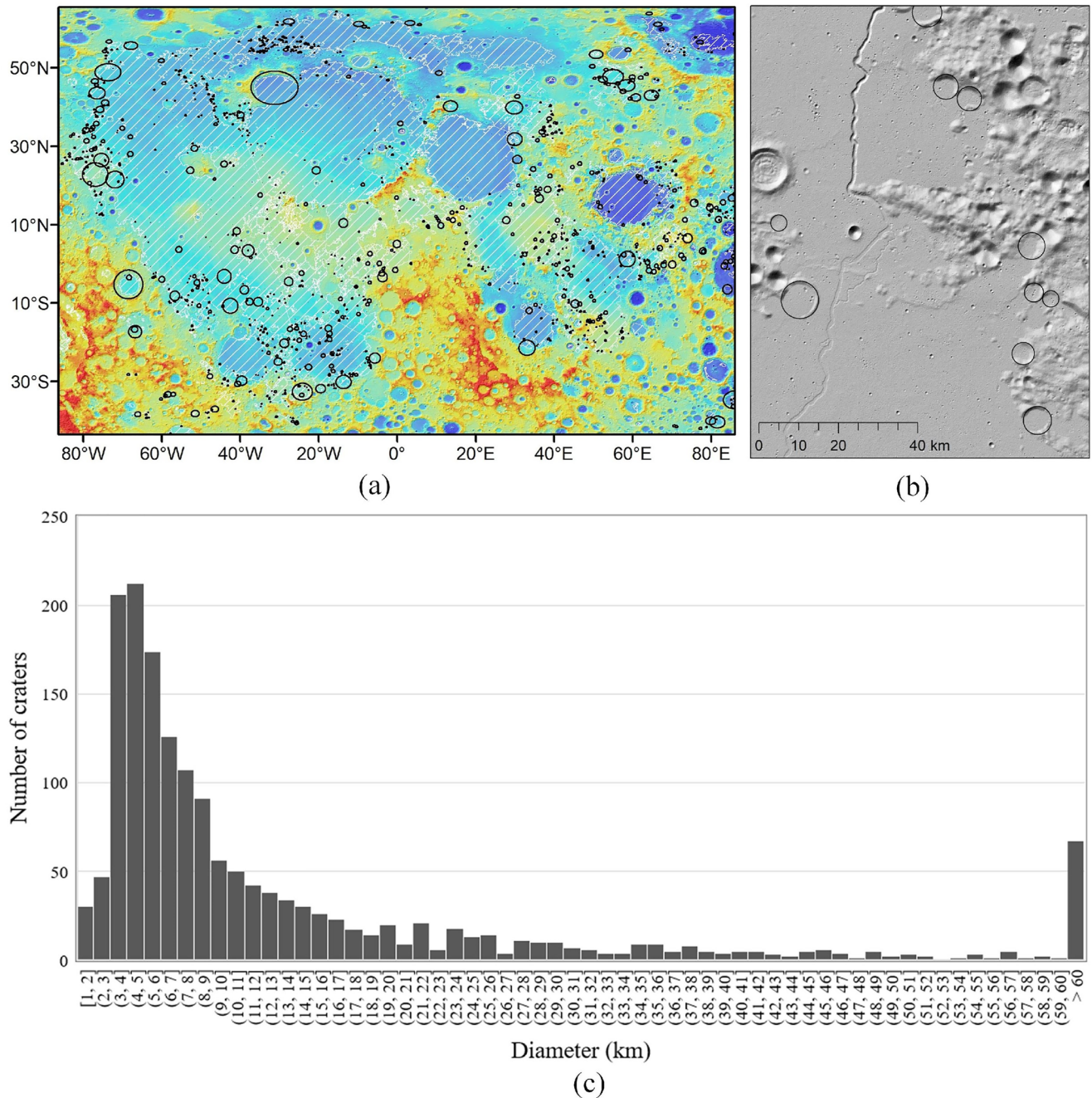


**Figure 5.** (a) Distribution of largely flooded craters (black outlines) on the main areas of lunar maria (marked by gray hatching). (b) Examples of flooded craters shown on a shaded relief of the SLDEM. (c) Histogram of all of the identified flooded craters in different diameter ranges.

The change in crater depth-to-diameter ratios with increasing crater size (Figure 4) may indicate the existence of a relatively weak upper layer and a competent underlying layer, with the turning point controlled by the depth of the interface between these two layers. Considering the crater depth, the weak upper layer referred to here is around several kilometers based on the above descriptions about the layered structure of the lunar crust, the weak upper layers here refer to the upper megaregolith for highlands and mare basalts for maria. In the highlands, this turning point occurs in craters with a diameter of 11–22 km, whereas in the lunar maria, it occurs in craters with a much smaller diameter of 8–16 km (after excluding the influence of basaltic flooding). As the turning points indicate the beginning of the crater penetrating the harder underlying layer, the depth of craters at the turning point can provide clues that enable the estimation of the thickness of the mare basalts and highland upper megaregolith.



To find the incipient crater diameters that penetrated to the harder, more competent underlying layer, we searched for the deepest simple craters in both the highlands and maria. In their nearby regions, larger craters with similar depths but flat floors were also identified. A comparison analysis of these two types of craters will allow us to estimate the depths of the upper layer at these regions.

Two simple craters in the lunar maria, Torricelli C and Alpetragius B, were identified and measured as shown in Figure 6. Torricelli C is located in the southern Mare Tranquillitatis and is bowl-shaped, with a diameter of  $\sim 10.6$  km and a depth of  $\sim 2.3$  km (a depth-to-diameter ratio of 0.22). Its diameter corresponds to the turning point from increasing to decreasing depth-to-diameter ratios for mare craters, as shown in Figure 4b. In its nearby region, the crater Hypatia A is also located in the southern Mare Tranquillitatis. Hypatia A is a flat-floored crater with a larger diameter ( $\sim 15.1$  km) but a similar depth ( $\sim 2.4$  km) to Torricelli C. The comparison between Torricelli C and Hypatia A indicates an upper limit of depth of  $\sim 2.4$  km for mare basalts in this region. The craters Alpetragius B and Kundt in northern Mare Nubium show similar cases, of which the former is a bowl-shaped (slightly flat-floored) crater with a diameter of  $\sim 9.2$  km and a depth of  $\sim 2.3$  km, but its nearby crater Kundt is obviously flat-floored with a slightly larger diameter of  $\sim 10.1$  km and a similar depth of  $\sim 2.3$  km.

Similar measurements were conducted in the lunar highlands. Regnault W, close to the northwest limb of the Moon, is the deepest simple crater we identified in the highlands. It has a diameter of  $\sim 14$  km and a depth of  $\sim 3.3$  km. Its nearby crater McLaughlin Z is flat-floored with a larger diameter ( $\sim 20.4$  km) but a similar depth ( $\sim 3.3$  km) as Regnault W. The craters Maander A and Lents J in the highlands also show similar patterns. Maander A is a bowl-shaped (slightly flat-floored) crater with a diameter of  $\sim 15.3$  km and a depth of  $\sim 3.2$  km. Its nearby crater Lents J has a similar diameter and a slightly larger depth but it is obviously flat-floored.

The deepest simple craters we identified on the lunar maria and highlands provide an approximate reference that these areas (where the deepest craters are located) have a thickness of up to  $\sim 2.3$  km for mare basalts and  $\sim 3.3$  km for highland upper megaregolith, respectively. It should be noted that the depths of layered structures are not homogenous throughout the lunar surface, and the estimated depths of mare basalts and highland upper megaregolith are from the sampling analyses of local regions. However, they provide a useful reference for similar studies in other regions.

The observed differences between the crater depth-to-diameter ratios of the lunar maria and those of the highlands may indicate differences between the properties of the target materials (e.g., Prieur et al., 2017; Senft & Stewart, 2007). Generally, crater morphologies can be influenced by target-rock strength (Collins et al., 2012), friction coefficient (Elbeshausen et al., 2009), porosity (Ding et al., 2018; Love et al., 1993; Milbury et al., 2015), and cohesion (Housen & Holsapple, 2011). According to numerical calculations, an increase in target-rock strength and friction coefficient decreases the crater depth (Collins et al., 2012; Elbeshausen et al., 2009); while compaction of porosity results in deeper craters (Love et al., 1993).

As shown in Figure 4b, for craters smaller than 16 km in diameter, median depth-to-diameter ratios of mare craters are larger than those of the highland craters (after excluding the influence of basaltic flooding on craters along mare-highland boundaries). Possible reasons for this include lower target strength (Collins et al., 2012), lower friction coefficient (Elbeshausen et al., 2009), and larger porosity (Love et al., 1993) for the mare basalts than the highland upper megaregolith. Considering the dependency of different target properties upon each other, it is likely that the mare basalts are more competent than the highland upper megaregolith.

#### 4. Conclusions and Discussion

Our analysis of the morphological characteristics of lunar impact craters on a global scale reveals the following findings:

1. There is a global power-law relationship with an offset term between crater depth-to-diameter ratios and crater densities for craters ( $\geq 1$  km in diameter) on the lunar surface, showing that deeper craters are located in younger surfaces with lower crater densities, and the average depth-to-diameter ratios of craters converge to  $\sim 0.07$  on saturated surfaces.
2. Small craters (less than  $\sim 4$  km in diameter) on the lunar maria are deeper than those on the highlands. Furthermore, after excluding the influence of basaltic flooding on craters along mare-highland boundaries,

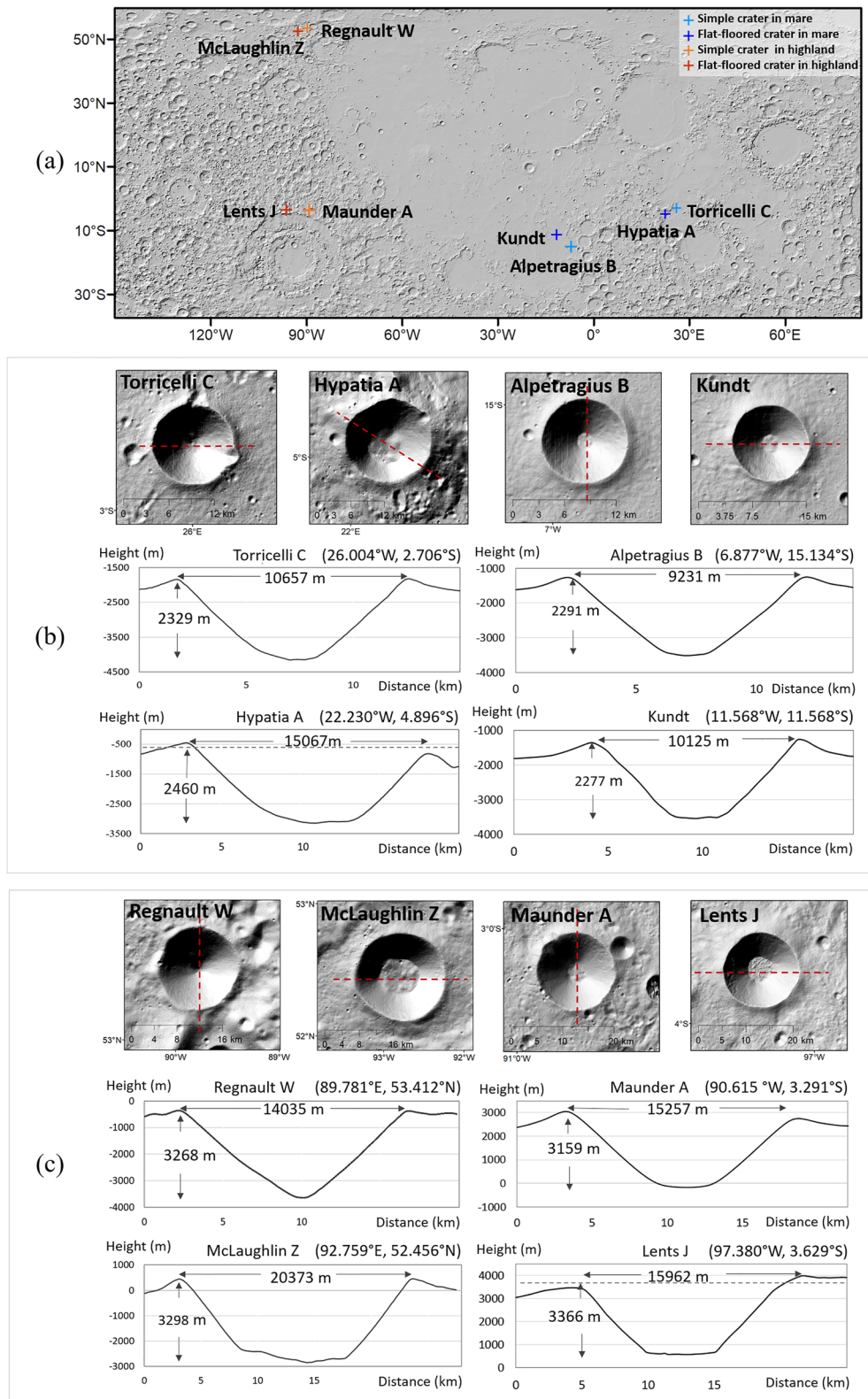


**Figure 6.** Examples of the deepest simple craters on the lunar maria and highlands and comparison with nearby flat-floored craters. (a) Distribution of the studied craters. (b) Simple craters and nearby flat-floored craters on maria and their elevation profiles (along the dashed red line). (c) Simple craters and nearby flat-floored craters on highlands and their elevation profiles.



the median depth-to-diameter ratios of mare craters remain greater than those of the highland craters in all of the binned ranges up to a diameter of 16 km.

3. The deepest simple craters identified on the lunar maria and highlands provide a reference that these regions have a thickness of up to  $\sim 2.3$  km for the mare basalts and  $\sim 3.3$  km for the highland upper megaregolith.

With the availability of 3D information on lunar impact craters ( $\geq 1$  km in diameter), we have the opportunity to explore the differences between the lunar maria and highlands in terms of crater degradation, the stratified layers, and the properties of the target materials, by using the crater morphology as a clue. The relationship between the crater morphology and these factors is complex and only a preliminary discussion is given in this paper. Numerical simulation of craters in basalt and anorthosite materials will help reveal further constraints on the findings of this paper, which will be our future efforts.

## Data Availability Statement

The crater catalog, LU1319373, has been made publicly available at Zenodo (<http://doi.org/10.5281/zenodo.4983248>). The SLDEM and LOLA DEMs are available from NASA's Planetary Data System (<https://pds-geosciences.wustl.edu/missions/lro/lola.htm>).

## Acknowledgments

This work was supported by grants from the Research grants Council of Hong Kong (RIF Project No: R5043-19, Project No: PolyU 15210520) and a grant from the National Natural Science Foundation of China (Project No: 41671426). The authors thank the individuals who helped make the archive of the data sets publicly available. The authors also thank Bob Craddock and an anonymous reviewer for their valuable comments that helped improve this study.

## References

- Aggarwal, H. R., & Oberbeck, V. R. (1979). Monte Carlo simulation of lunar megaregolith and implications. In *Lunar and Planetary Science Conference Proceedings* (Vol. 10, pp. 2689–2705).
- Baldwin, R. B. (1970). *A new method of determining the depth of the lava in lunar maria* (pp. 857–864). Publications of the Astronomical Society of the Pacific.
- Barker, M., Mazarico, E., Neumann, G., Zuber, M., Haruyama, J., & Smith, D. (2016). A new lunar digital elevation model from the Lunar Orbiter Laser Altimeter and SELENE Terrain Camera. *Icarus*, 273, 346–355. <https://doi.org/10.1016/j.icarus.2015.07.039>
- Barnouin, O. S., Zuber, M. T., Smith, D. E., Neumann, G. A., Herrick, R. R., Chappelow, J. E., et al. (2012). The morphology of craters on Mercury: Results from MESSENGER flybys. *Icarus*, 219(1), 414–427. <https://doi.org/10.1016/j.icarus.2012.02.029>
- Basilevsky, A. T., Kozlova, N. A., Zavyalov, I. Y., Karachevtseva, I. P., & Kreslavsky, M. A. (2018). Morphometric studies of the Copernicus and Tycho secondary craters on the Moon: Dependence of crater degradation rate on crater size. *Planetary and Space Science*, 162, 31–40. <https://doi.org/10.1016/j.pss.2017.06.001>
- Collins, G. S., Melosh, H. J., & Osinski, G. R. (2012). The impact-cratering process. *Elements*, 8(1), 25–30. <https://doi.org/10.2113/gselements.8.1.25>
- De Hon, R. A. (1974). Thickness of mare material in the Tranquillitatis and Nectaris basins. In *Lunar and Planetary Science Conference Proceedings* (Vol. 5, pp. 53–59).
- De Hon, R. A. (1975). Mare Spumans and Mare Undarum-Mare thickness and basin floor. In *Lunar and Planetary Science Conference Proceedings* (Vol. 6, pp. 2553–2561).
- De Hon, R. A. (1977). Mare Humorum and Mare Nubium-Basalt thickness and basin-forming history. In *Lunar and Planetary Science Conference Proceedings* (Vol. 8, pp. 633–641).
- Ding, M., Soderblom, J. M., Bierson, C. J., Nimmo, F., Milbury, C., & Zuber, M. T. (2018). Constraints on lunar crustal porosity from the gravitational signature of impact craters. *Journal of Geophysical Research: Planets*, 123(9), 2281–2294. <https://doi.org/10.1029/2018je005654>
- Du, J., Fa, W., Wiczorek, M. A., Xie, M., Cai, Y., & Zhu, M. (2019). Thickness of lunar mare basalts: New results based on modeling the degradation of partially buried craters. *Journal of Geophysical Research: Planets*, 124(9), 2430–2459. <https://doi.org/10.1029/2018je005872>
- Elbeshhausen, D., Wünnemann, K., & Collins, G. S. (2009). Scaling of oblique impacts in frictional targets: Implications for crater size and formation mechanisms. *Icarus*, 204(2), 716–731. <https://doi.org/10.1016/j.icarus.2009.07.018>
- Fassett, C., Crowley, M. C., Leight, C., Dyar, M. D., Minton, D., Hirabayashi, M., et al. (2017). Using measurements of topography to infer rates of crater degradation and surface evolution on the Moon and Mercury. In *AGU Fall Meeting Abstracts* (Vol. 2017, P24C-01).
- Fassett, C. I., & Combellick, J. R. (2014). The rate of crater degradation and topographic evolution on the Moon: Results from the maria and initial comparisons with the highlands. In *Lunar and Planetary Science Conference* (Vol. 1777, p. 1429).
- Fassett, C. I., & Thomson, B. J. (2014). Crater degradation on the lunar maria: Topographic diffusion and the rate of erosion on the Moon. *Journal of Geophysical Research: Planets*, 119(10), 2255–2271. <https://doi.org/10.1002/2014je004698>
- Gong, S., Wiczorek, M. A., Nimmo, F., Kiefer, W. S., Head, J. W., Huang, C., et al. (2016). Thicknesses of mare basalts on the Moon from gravity and topography. *Journal of Geophysical Research: Planets*, 121(5), 854–870. <https://doi.org/10.1002/2016je005008>
- Head, J. W. (1982). Lava flooding of ancient planetary crusts: Geometry, thickness, and volumes of flooded lunar impact basins. *The Moon and the Planets*, 26(1), 61–88. <https://doi.org/10.1007/bf00941369>
- Head, J. W., Fassett, C. I., Kadish, S. J., Smith, D. E., Zuber, M. T., Neumann, G. A., & Mazarico, E. (2010). Global distribution of large lunar craters: Implications for resurfacing and impactor populations. *Science*, 329(5998), 1504–1507. <https://doi.org/10.1126/science.1195050>
- Housen, K. R., & Holsapple, K. A. (2011). Ejecta from impact craters. *Icarus*, 211(1), 856–875. <https://doi.org/10.1016/j.icarus.2010.09.017>
- Izquierdo, K., Sori, M. M., Soderblom, J. M., Johnson, B. C., & Wiggins, S. E. (2021). Lunar megaregolith structure revealed by GRAIL gravity data. *Geophysical Research Letters*, 48(22), e2021GL095978. <https://doi.org/10.1029/2021gl095978>
- Kalynn, J., Johnson, C. L., Osinski, G. R., & Barnouin, O. (2013). Topographic characterization of lunar complex craters. *Geophysical Research Letters*, 40(1), 38–42. <https://doi.org/10.1029/2012gl053608>
- Kato, M., Sasaki, S., Tanaka, K., Iijima, Y., & Takizawa, Y. (2008). The Japanese lunar mission SELENE: Science goals and present status. *Advances in Space Research*, 42(2), 294–300. <https://doi.org/10.1016/j.asr.2007.03.049>
- Li, C., Liu, X., Ren, X., Yan, W., Zuo, W., Mu, L., et al. (2018). Lunar global high-precision terrain reconstruction based on Chang'e-2 stereo images. *Wuhan Daxue Xuebao*, 43, 485–495.

- Love, S. G., Hörz, F., & Brownlee, D. E. (1993). Target porosity effects in impact cratering and collisional disruption. *Icarus*, 105(1), 216–224. <https://doi.org/10.1006/icar.1993.1119>
- Melosh, H. J. (1977). Crater modification by gravity: A mechanical analysis of slumping. In D. J. Roddy, R. O. Pepin, & R. B. Merrill (Eds.), *Impact and explosion cratering* (pp. 1245–1260). Pergamon Press.
- Melosh, H. J. (1989). *Impact cratering: A geologic process*. Oxford University Press.
- Milbury, C., Johnson, B. C., Melosh, H. J., Collins, G. S., Blair, D. M., Soderblom, J. M., et al. (2015). Preimpact porosity controls the gravity signature of lunar craters. *Geophysical Research Letters*, 42(22), 9711–9716. <https://doi.org/10.1002/2015gl066198>
- Neukum, G., Ivanov, B. A., & Hartmann, W. K. (2001). Cratering records in the inner solar system in relation to the lunar reference system. *Chronology and Evolution of Mars*, 96(1/4), 55–86. <https://doi.org/10.1023/a:1011989004263>
- Oberbeck, V. R., & Quaide, W. L. (1968). Genetic implications of lunar regolith thickness variations. *Icarus*, 9(1–3), 446–465. [https://doi.org/10.1016/0019-1035\(68\)90039-0](https://doi.org/10.1016/0019-1035(68)90039-0)
- Pike, R. J. (1974). Depth/diameter relations of fresh lunar craters: Revision from spacecraft data. *Geophysical Research Letters*, 1(7), 291–294. <https://doi.org/10.1029/gl001i007p00291>
- Pike, R. J. (1981). Target-dependence of crater depth on the Moon. *Lunar and Planetary Science Conference Proceedings* (pp. 845–847).
- Pike, R. J., & Spudis, P. D. (1987). Basin-ring spacing on the Moon, Mercury, and Mars. *Earth, Moon, and Planets*, 39(2), 129–194. <https://doi.org/10.1007/bf00054060>
- Prieur, N. C., Rolf, T., Luther, R., Wünnemann, K., Xiao, Z., & Werner, S. C. (2017). The effect of target properties on transient crater scaling for simple craters. *Journal of Geophysical Research: Planets*, 122(8), 1704–1726. <https://doi.org/10.1002/2017je005283>
- Richardson, J. E. (2009). Cratering saturation and equilibrium: A new model looks at an old problem. *Icarus*, 204(2), 697–715. <https://doi.org/10.1016/j.icarus.2009.07.029>
- Richardson, J. E., & Abramov, O. (2020). Modeling the formation of the lunar upper megaregolith layer. *The Planetary Science Journal*, 1(1), 2. <https://doi.org/10.3847/psj/ab7235>
- Robbins, S. J. (2019). A new global database of lunar impact craters > 1–2 km: Crater locations and sizes, comparisons with published databases, and global analysis. *Journal of Geophysical Research: Planets*, 124(4), 871–892. <https://doi.org/10.1029/2018je005592>
- Schultz, P. H., Greeley, R., & Gault, D. (1977). Interpreting statistics of small lunar craters. In *Lunar Science Conference Proceedings*.
- Senft, L. E., & Stewart, S. T. (2007). Modeling impact cratering in layered surfaces. *Journal of Geophysical Research*, 112, E11. <https://doi.org/10.1029/2007je002894>
- Smith, D. E., Zuber, M. T., Neumann, G. A., Lemoine, F. G., Mazarico, E., Torrence, M. H., et al. (2010). Initial observations from the Lunar Orbiter Laser Altimeter (LOLA). *Geophysical Research Letters*, 37(18), L18204. <https://doi.org/10.1029/2010gl043751>
- Thomson, B. J., Grosfils, E. B., Bussey, D. B. J., & Spudis, P. D. (2009). A new technique for estimating the thickness of mare basalts in Imbrium Basin. *Geophysical Research Letters*, 36(12), L12201. <https://doi.org/10.1029/2009gl037600>
- Wang, Y., & Wu, B. (2019). Active machine learning approach for crater detection from planetary imagery and digital elevation models. *IEEE Transactions on Geoscience and Remote Sensing*, 57(8), 5777–5789. <https://doi.org/10.1109/tgrs.2019.2902198>
- Wang, Y., Wu, B., Xue, H., Li, X., & Ma, J. (2021). An improved global catalog of lunar impact craters ( $\geq 1$  km) with 3D morphometric information and updates on global crater analysis. *Journal of Geophysical Research: Planets*, 126(9), e2020JE006728. <https://doi.org/10.1029/2020je006728>
- Werner, S. C. (2014). Moon, Mars, Mercury: Basin formation ages and implications for the maximum surface age and the migration of gaseous planets. *Earth and Planetary Science Letters*, 400, 54–65. <https://doi.org/10.1016/j.epsl.2014.05.019>
- Whitford-Stark, J. L. (1982). A preliminary analysis of lunar extra-mare basalts: Distribution, compositions, ages, volumes, and eruption styles. *The Moon and the Planets*, 26(3), 323–338. <https://doi.org/10.1007/bf00928015>
- Wiggins, S. E., Johnson, B. C., Bowling, T. J., Melosh, H. J., & Silber, E. A. (2019). Impact fragmentation and the development of the deep lunar megaregolith. *Journal of Geophysical Research: Planets*, 124(4), 941–957. <https://doi.org/10.1029/2018je005757>
- Wood, C., & Anderson, L. (1978). New morphometric data for fresh lunar craters. *Lunar and Planetary Science Conference Proceedings* (pp. 3669–3689).
- Woronow, A. (1977a). Crater saturation and equilibrium: A Monte Carlo simulation. *Journal of Geophysical Research*, 82(17), 2447–2456. <https://doi.org/10.1029/jb082i017p02447>
- Woronow, A. (1977b). A simulation of the lunar highlands crater population [Technical Report]. In: *Lunar and Planetary Institute Conference*, (Vol. 8 p. 1032).
- Woronow, A. (1978). A general cratering-history model and its implications for the lunar highlands. *Icarus*, 34(1), 76–88. [https://doi.org/10.1016/0019-1035\(78\)90127-6](https://doi.org/10.1016/0019-1035(78)90127-6)
- Wünnemann, K., & Ivanov, B. (2003). Numerical modelling of the impact crater depth–diameter dependence in an acoustically fluidized target. *Planetary and Space Science*, 51(13), 831–845. <https://doi.org/10.1016/j.pss.2003.08.001>
- Xiao, Z., & Werner, S. C. (2015). Size-frequency distribution of crater populations in equilibrium on the Moon. *Journal of Geophysical Research: Planets*, 120(12), 2277–2292. <https://doi.org/10.1002/2015je004860>
- Yue, Z., Di, K., Liu, Z., Michael, G., Jia, M., Xin, X., et al. (2019). Lunar regolith thickness deduced from concentric craters in the CE-5 landing area. *Icarus*, 329, 46–54. <https://doi.org/10.1016/j.icarus.2019.03.032>